Journal of Alloys and Compounds 504S (2010) S98–S101

Contents lists available at ScienceDirect

Journal of Alloys and Compounds

journal homepage: www.elsevier.com/locate/jallcom

Improvement of mechanical properties in MgCuYNdAg bulk metallic glasses with adding Mo particles

P.J. Hsieh*, L.C. Yang, H.C. Su, C.C. Lu, J.S.C. Jang

Department of Materials Science and Engineering, I-Shou University, No. 1, Sec. 1, Syuecheng Rd., Dashu Township, Kaohsiung 84001, Taiwan, ROC

ARTICLE INFO

Article history:
Received 3 July 2009
Received in revised form 10 April 2010
Accepted 14 April 2010
Available online 20 April 2010

Keywords:
Metallic glasses
Toughness
Mg-based BMGC

ABSTRACT

In this study, the $Mg_{58}Cu_{29.5}Y_6Nd_5Ag_{1.5}$ bulk metallic glasses (BMGs) with superior glass forming ability are made by Cu-mold casting and injection casting processes. Critical rod size of the $Mg_{58}Cu_{29.5}Y_6Nd_5Ag_{1.5}$ BMGs (base alloys) reached ~4 mm in diameter. The results of Vickers indentation and compression tests of $Mg_{58}Cu_{29.5}Y_6Nd_5Ag_{1.5}$ alloy reveal that the mechanical performance of the BMG base alloy is brittle. The highest fracture toughness and plastic strain of the base alloy are only ~9 MPa $m^{1/2}$ and ~0%, respectively. SEM observation is followed after the mechanical properties tests. It showed that the dominant patterns of the fracture surface are the featureless mirror-like and river-like regions. For enhancing the mechanical properties of the base alloys, porous Mo particles are added to form $Mg_{58}Cu_{29.5}Y_6Nd_5Ag_{1.5}$–Mo BMG composites (BMGCs). It is found that the fracture toughness and the fracture strength of the 30 vol.% Mo particles reinforced $Mg_{58}Cu_{29.5}Y_6Nd_5Ag_{1.5}$ BMGCs is promoted to ~50 MPa $m^{1/2}$ and ~1100 MPa. The observation of the fracture surface of $Mg_{58}Cu_{29.5}Y_6Nd_5Ag_{1.5}$–30 vol.% Mo BMG composite via the compression test reveals that the shear bands and cracks propagation is resisted by the dispersion of Mo particles and secondary shear bands are formed during the plastic deformation. It is also observed that the fracture surface is occupied by vein-like pattern, instead of mirror-like region. Moreover, the plastic strain of the $Mg_{58}Cu_{29.5}Y_6Nd_5Ag_{1.5}$–30 vol.% Mo BMG composite increased to ~29%.

1. Introduction

As compared with the traditional crystalline alloys, bulk metallic glasses with the short-range or random atomic ordering have been paid worldwide attentions due to their unique mechanical properties, such as high compressive fracture strength, hardness, and good corrosion resistance [1–4]. Among bulk metallic glasses, the lightweight Mg-based alloys (the specific weight for Mg is 1.7 g/cm^3), such as Mg–Cu–RE–TM (RE: rare earth metal, such as Y, Gd, Nd and Tb; TM: transition metal) BMGs [5–9], with high glass forming ability (GFA) and large supercooled liquid region are of interest for the resource shortage and environment contamination problems. However the brittle fracture behavior and low plasticity of BMGs at room temperature limited their potential in application, especially for the Mg-based alloys. Hence, numerous efforts have been made to solve the low ductility problems of Mg-based BMGs. Recently, the most attractive and effective way to enhance the room-temperature plasticity of BMGs were focused on the ex situ method. To improve the mechanical properties of BMGs by the ex situ method, bulk metallic glass composites (BMGCs) are synthesized by the introducing of various metallic or ceramic second phase particles (e.g., TiB_2 [10], ZrO_2 [11], WC [12], SiC [13], Nb [14], Mo [15], and Ti [16]) into the BMG matrix alloys. Many kinds of Mg-based BMGs have been used to form the bulk metallic glass composites by following this idea. Previous studies revealed that the dispersion of micrometer or nanometer size crystalline particles in the amorphous matrix leads to the serrated flow of shear bands and the retarded crack propagation. Hence, the remarkable macroscopic plasticity promotions of the BMGCs were observed. For example, the $Mg_{65}Cu_{25}Gd_{10}$ BMGC with adding 40 vol.% Ti exhibits ~40% plastic strain [16]. It is suggested that the mechanical properties of BMGCs increased with increasing volume fraction of second phase particles. Besides, it has also been reported that the yield strength or the glass forming ability of BMGCs may decrease depending on the category of the reinforcements.

In order to explore the effects of the adding of second phase particles on the mechanical properties of BMGs, the $Mg_{58}Cu_{29.5}Y_6Nd_5Ag_{1.5}$ alloy with high glass forming ability was selected as the base material in this research. The micro-addition of Ag, which has a large negative heat of mixing with Mg and Cu, had also been certified to be effective to promote GFA and thermal stability of Mg-based BMGs [15]. Porous Mo particles with large amount, 20, 25 and 30 vol.%, were doped in the base alloys. The selection of Mo as the reinforced particles in BMG matrix was based on the following reason: Mo particle is stable and insoluble in the Mg-based BMG matrix and it exhibits high melting

* Corresponding author. Tel.: +886 7 6577711x3120; fax: +886 7 6578444.
E-mail address: pjhsieh@isu.edu.tw (P.J. Hsieh).

0925-8388/$ – see front matter © 2010 Elsevier B.V. All rights reserved.
doi:10.1016/j.jallcom.2010.04.066

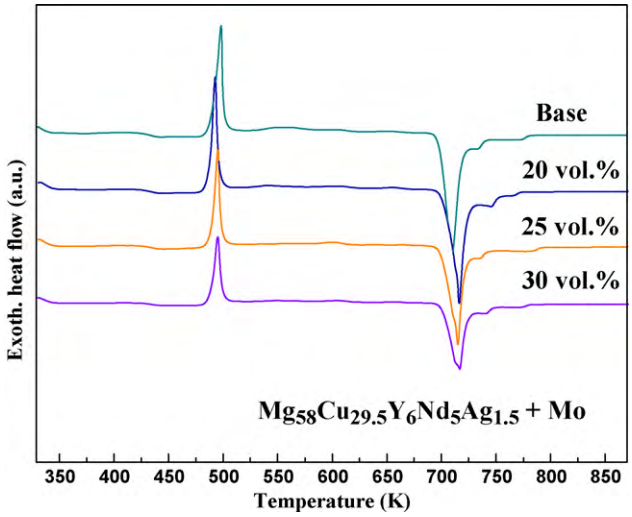

Fig. 1. DSC traces of $Mg_{58}Cu_{29.5}Y_6Nd_5Ag_{1.5}$ BMGCs with adding 0 vol.%, 20 vol.%, 25 vol.% and 30 vol.% Mo particles.

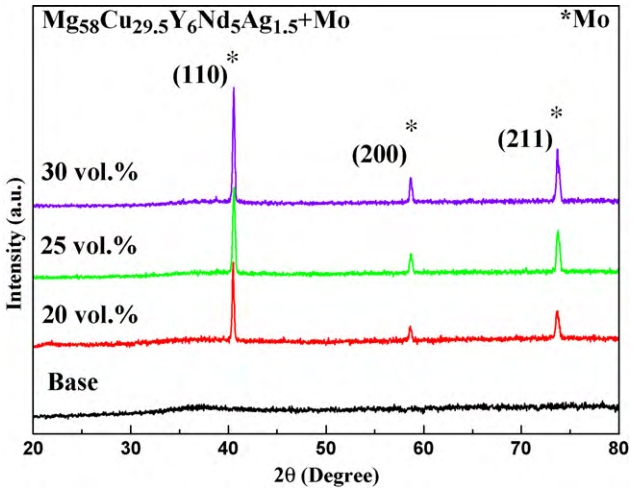

Fig. 2. X-ray diffraction patterns of $Mg_{58}Cu_{29.5}Y_6Nd_5Ag_{1.5}$ BMGCs with adding 0 vol.%, 20 vol.%, 25 vol.% and 30 vol.% Mo particles.

temperature and elastic modulus (near to the value of 2890 K and 327 GPa, respectively) [15]. The effects of the dispersion strengthening mechanism on the mechanical property improvement of the brittle Mg-based BMGCs are discussed in this paper.

2. Experimental procedures

Alloy ingots with the selected composition $Mg_{58}Cu_{29.5}Y_6Nd_5Ag_{1.5}$ were made from elemental metals with purity ~99.9 at.%. First, the CuYNdAg ingot was pre-alloyed by the arc melting method under a Ti-gettered argon atmosphere. Then the CuYNdAg intermediate alloy was re-melted with the Mg pieces to obtain the base material by the induction melting process. Afterwards, the reinforced particles were mixed with the melted base alloy by using a mechanical stirring process to develop the $Mg_{58}Cu_{29.5}Y_6Nd_5Ag_{1.5}$ BMGCs with different volume fractions (20, 25 and 30 vol.%) of Mo powders addition. Furthermore, the BMGCs sample rods with the diameter in the range of 2–5 mm and the length of 50 mm were produced by water-cooled Cu-mold injection casting process.

Thermal properties and the amorphous structure of $Mg_{58}Cu_{29.5}Y_6Nd_5Ag_{1.5}$ BMG (base alloy) and BMGCs with various Mo contents were examined by using differential scanning calorimeter (TA instruments DSC 2920) at a heating rate of 20 K/min and X-ray diffraction (Scintag X-400 diffractometer) with monochromatic Cu Kα radiation. The uniaxial compression tests (specimen size was 2 mm in diameter and 4 mm in height) were performed to evaluate the mechanical properties of BMG alloys by a MTS 810 mechanical test system at a strain rate of $5 \times 10^{-4}\ s^{-1}$ under room temperature. Hardness and fracture toughness of base alloy and BMGCs were measured by macro-Vickers hardness tester (Akashi MVK-H11) with the load in the range of 5–30 kg. The morphology and the microstructures of the fracture specimens were analyzed with a field-emission scanning electric microscopy (FE-SEM, Hitachi S-4700) with energy dispersive spectrometry (EDS) capability.

3. Results and discussions

Fig. 1 shows the DSC traces of $Mg_{58}Cu_{29.5}Y_6Nd_5Ag_{1.5}$ BMG base alloy and BMGCs with 20, 25 and 30 vol.% of Mo particles, and the basic thermal properties extracted from the DSC scanning curves are summarized in Table 1. The glass forming ability (GFA) parameters, $T_{rg}(=T_g/T_l)$, $\gamma(=T_x/(T_g+T_l))$ and $\gamma_m(=(2T_x-T_g)/T_l)$, are also estimated and listed in Table 1. Slightly decreasing of T_x with the increasing of Mo content, and so was the supercooled liquid region (ΔT_x) of Mg-based BMGCs. However, the $Mg_{58}Cu_{29.5}Y_6Nd_5Ag_{1.5}$ BMGCs with adding 30 vol.% of Mo particles maintained high glass forming ability (γ_m value ~0.76) due to the insolubility of Mo particles and Mg-based BMG matrix. Fig. 2 shows the XRD patterns of $Mg_{58}Cu_{29.5}Y_6Nd_5Ag_{1.5}$ base alloy and BMGCs with the addition of 20, 25 and 30 vol.% Mo particles. Except for the broadening peaks diffracted from the typical amorphous structure, only three crystalline peaks derived from the Mo particles can be resolved in the XRD patterns of Mg-based BMGCs. No obvious chemical reaction is detected. It indicated that the addition of Mo particles does not change the amorphous structure of the base alloy, due to the immiscible feature of bcc-Mo particles with the BMG matrix. This characteristic is also confirmed by the typical SEM/EDS measurements of Mg-based base alloy and BMGCs. The EDS results showed that the composition of the matrix around Mo particles dispersed in BMGCs is very close to that of the base alloys. Only a small composition range (56–58% Mg, 29–30% Cu, 5–7% Y, 5–6% Nd and 1.5% Ag) can be observed.

Uniaxial compressive tests and Vickers hardness indentations are conducted at room temperature to explore the additive effect of the Mo particles on the mechanical properties of $Mg_{58}Cu_{29.5}Y_6Nd_5Ag_{1.5}$–Mo alloys. Fig. 3 reveals the true stress–strain curve of the studied Mg-based BMGCs subjected to the

Table 1
Thermal properties of $Mg_{58}Cu_{29.5}Y_6Nd_5Ag_{1.5}$ BMGCs with adding 0 vol.%, 20 vol.%, 25 vol.% and 30 vol.% Mo particles.

	T_g (K)	T_x (K)	T_l (K)	ΔT_x (K)	T_{rg}	γ	γ_m
Base	420	490	718	70	0.59	0.43	0.78
20 vol.%	422	488	722	66	0.58	0.43	0.77
25 vol.%	424	489	724	65	0.58	0.43	0.77
30 vol.%	422	483	721	61	0.58	0.42	0.76

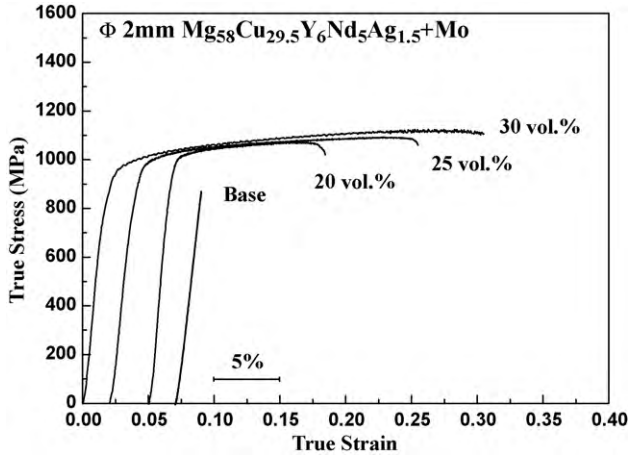

Fig. 3. True stress–strain curves of $Mg_{58}Cu_{29.5}Y_6Nd_5Ag_{1.5}$ BMGCs with adding 0 vol.%, 20 vol.%, 25 vol.% and 30 vol.% Mo particles subjected to the room-temperature compressive tests.

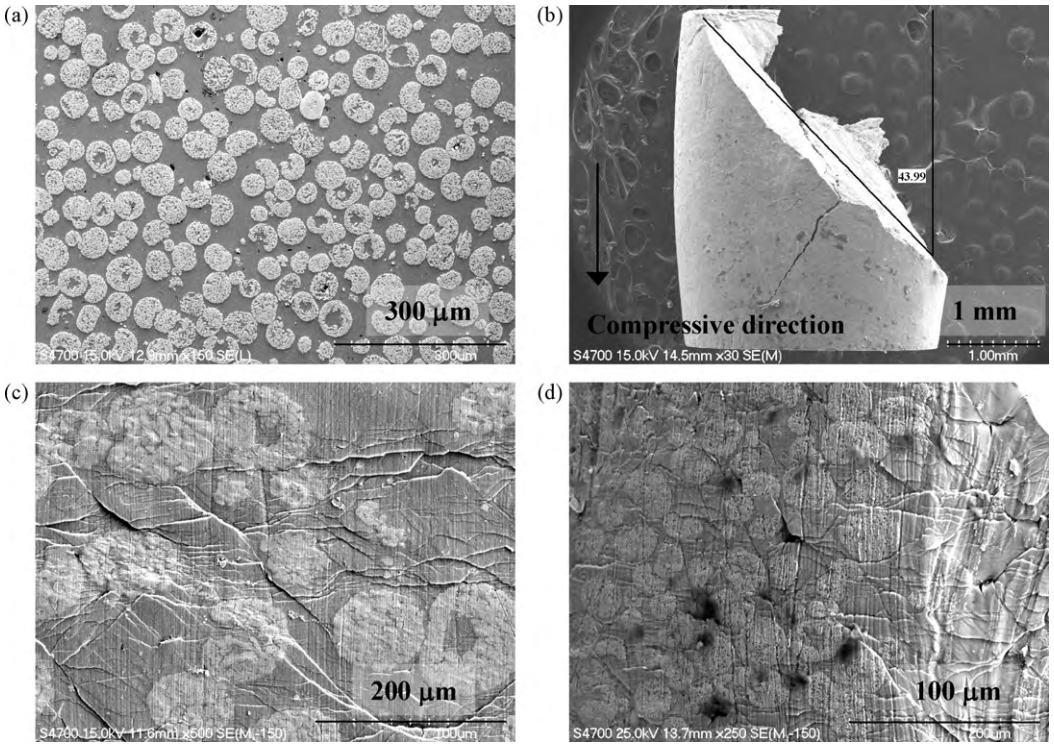

Fig. 4. SEM images of $Mg_{58}Cu_{29.5}Y_6Nd_5Ag_{1.5}$ BMGCs with adding 30 vol.% Mo particles taken from (a) the cross-section of rod specimen, (b) the overall fractured specimen, (c) the outer appearance on the side area near the fracture surface and (d) is the enlarge image of (c).

room-temperature compressive tests. The $Mg_{58}Cu_{29.5}Y_6Nd_5Ag_{1.5}$ with adding 20 vol.% Mo displays 12% plastic strain, which is twice higher than that of $Mg_{58}Cu_{29.5}Y_6Nd_5$–20 vol.% Mo [15]. It indicated that the micro-addition of Ag in MgCuYNd alloy systems contributes to the plasticity enhancement of BMGs. Meanwhile, the $Mg_{58}Cu_{29.5}Y_6Nd_5Ag_{1.5}$–30 vol.% Mo exhibits large plastic strain of 29% accompanying with high yield stress ($\sigma_y \sim 1003$ MPa) and ultimate compression stress ($\sigma_f \sim 1124$ MPa). As compared with the mechanical properties (also shown in Table 2) of base alloy, the addition of Mo particles has greatly contributed to the improvement of room-temperature macroscopic plasticity. Strength of the Mo particles reinforced Mg-based BMGCs increased with increasing Mo content. To clarify the strengthening mechanism of Mo additive in $Mg_{58}Cu_{29.5}Y_6Nd_5Ag_{1.5}$ BMGs, SEM analyses of the deformed specimens via compressive tests are followed. Fig. 4(a) shows the SEM image of the cross-section of the $Mg_{58}Cu_{29.5}Y_6Nd_5Ag_{1.5}$ rod with 30 vol.% of Mo particles. It reveals that the average size of porous Mo particles is about 50 μm and the Mo powders are dispersed in the amorphous matrix homogeneously. The dispersion strengthening mechanism of Mg-based BMGC is obtained when the additive hard phase is uniformly distributed in the matrix. Furthermore, the SEM observation of the outer surface of the fractured BMGC sample with 30 vol.% Mo content that undergoes compression test at room temperature is shown in Fig. 4(b). The fracture surface of BMGC sample with 30 vol.% Mo is observed to be inclined at ~45° to the compressive axis. Fig. 4(c) and (d) shows the SEM images of outer appearance on the side area near the fracture surface. Two kinds of shear bands can be observed in these figures. Primary shear band is perpendicular to and the other is paralleled to the normal direction of fracture surface. The propagation of shear bands during plastic deformation is impeded by the dense dispersion of Mo particles. It caused the progressing shear bands bended and branched to form multiple shear bands in order to bypass the strong dispersoid, Mo.

Table 2
Mechanical properties of $Mg_{58}Cu_{29.5}Y_6Nd_5Ag_{1.5}$ BMGCs with adding 0 vol.%, 20 vol.%, 25 vol.% and 30 vol.% Mo particles.

	σ_y (MPa)	σ_f (MPa)	ε_p (%)	H_v	K_c (MPa m$^{1/2}$)
Base	866	866	0	306 ± 6	15 ± 2
20 vol.%	1014	1071	12.2	316 ± 7	35 ± 4
25 vol.%	1016	1091	22.9	330 ± 10	40 ± 6
30 vol.%	1003	1124	29.1	342 ± 12	51 ± 2

Fig. 5 shows the SEM images examined on the fracture surfaces of $Mg_{58}Cu_{29.5}Y_6Nd_5Ag_{1.5}$ base alloy and BMGCs with containing 30 vol.% Mo via compression tests. The fracture surface of $Mg_{58}Cu_{29.5}Y_6Nd_5Ag_{1.5}$ base alloy is dominated by the featureless mirror-like images, indicating that the fracture mode of base alloy is brittle. It leads to the suddenly failure behavior of base alloys before yielding. However, the fracture surface of BMGCs-30 vol.% Mo is occupied by vein-like pattern the vein-like pattern instead, which is the characteristic of plastic deformation behavior of bulk metallic glasses.

The hardness and the fracture toughness of $Mg_{58}Cu_{29.5}Y_6Nd_5Ag_{1.5}$ BMGCs are measured by the Vickers indentation method [17] and the results are summarized in Table 2. It demonstrated that the hardness and the fracture toughness increased with the increasing of the volume fraction of Mo particles. Fig. 6 shows the SEM images of Vickers indentation on $Mg_{58}Cu_{29.5}Y_6Nd_5Ag_{1.5}$ base alloy and BMGCs with containing 30 vol.% Mo, which displays that some cracks emanated from the impression corners under a static load of 30 kg. By using Vickers indentation fracture (VIF) technique, the length of extended cracks can be adopted to evaluate fracture toughness (K_c) of the desired alloys. It seems that the additive particles improved the fracture toughness of the studied alloys. The $Mg_{58}Cu_{29.5}Y_6Nd_5Ag_{1.5}$ BMGCs with the addition of 30 vol.% Mo presents a high fracture toughness of ~51 MPa m$^{1/2}$. This result corresponds with that of compressive tests.

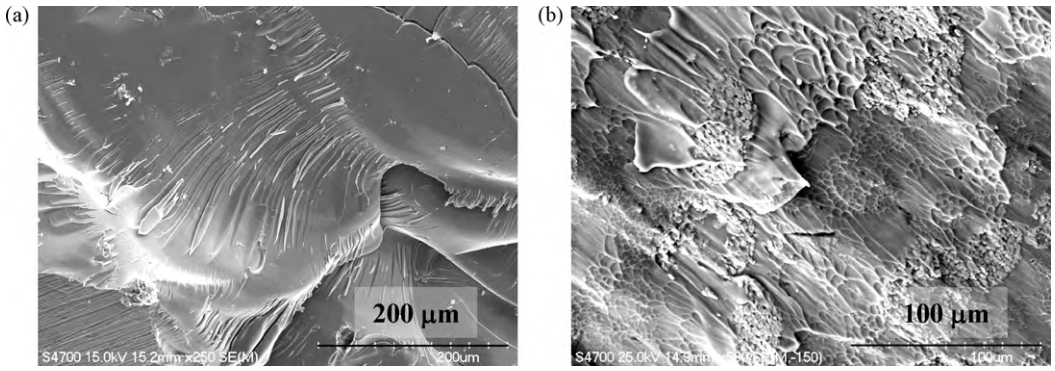

Fig. 5. SEM observations on the fracture surface of $Mg_{58}Cu_{29.5}Y_6Nd_5Ag_{1.5}$: (a) base alloy and (b) BMGC with 30 vol.% Mo.

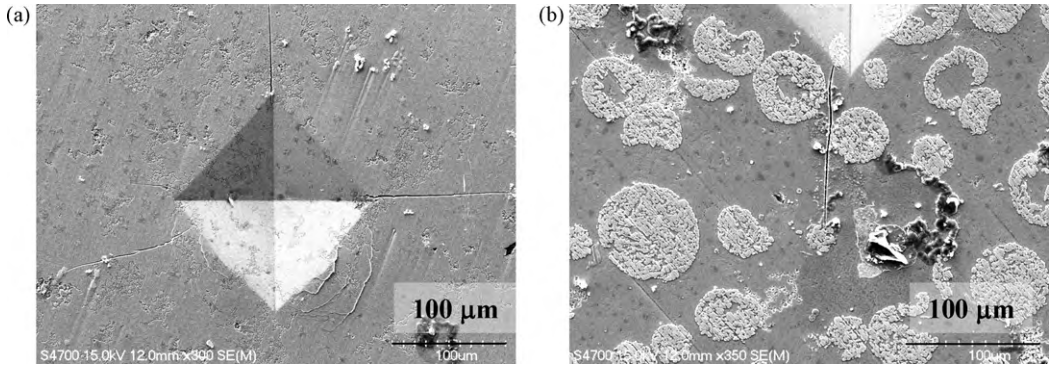

Fig. 6. SEM micrographs of Vickers indentation on $Mg_{58}Cu_{29.5}Y_6Nd_5Ag_{1.5}$: (a) base alloy and (b) BMGC with 30 vol.% Mo.

4. Conclusions

The $Mg_{58}Cu_{29.5}Y_6Nd_5Ag_{1.5}$ BMGCs with containing 30 vol.% Mo shows a high plastic strain and fracture strength of 29% and 1124 MPa, respectively. The micro-addition of Ag and the induction of reinforced Mo particles constitute the notable plasticity improvement of MgCuYNd BMGs. Mechanical properties of $Mg_{58}Cu_{29.5}Y_6Nd_5Ag_{1.5}$ BMGCs increased with increasing Mo content. Due to the insoluble characteristic of Mo in the Mg-based alloy, the addition of Mo particles does not cause critical change of thermal properties of BMG base alloys. Besides, the dense dispersion of the Mo particles in the amorphous matrix retarded the propagation of shear bands and resulted in the formation of multiple shear bands. Hence, it offers effective toughening mechanism of MgCuYNd BMGs.

Acknowledgements

The authors are gratefully acknowledge the sponsorship by National Science Council of Taiwan (R.O.C.) under the project no. NSC 95-2221-E-214-016-MY3 and the Micro- and Nano-Structure Analysis Lab in I-Shou university.

References

[1] A. Inoue, K. Ohtera, K. Kita, T. Masumoto, Jpn. J. Appl. Phys. 27 (1988) L2248.
[2] A. Inoue, T. Masumoto, Mater. Sci. Eng. A 173 (1993) 1.
[3] A. Inoue, A. Kato, T. Zhang, S.G. Kim, T. Masumoto, Mater. Trans., JIM 32 (1991) 609.
[4] A. Inoue, T. Nakamura, N. Nishiyama, T. Masumoto, Mater. Trans., JIM 33 (1992) 937.
[5] Y.K. Xu, J. Xu, Scripta Mater. 49 (2003) 843.
[6] H. Ma, Q. Zheng, J. Xu, Y. Li, E. Ma, J. Mater. Res. 20 (2005) 2252.
[7] H. Ma, L.L. Shi, J. Xu, Y. Li, E. Ma, J. Mater. Res. 21 (2006) 61.
[8] Q. Zheng, H. Ma, E. Ma, J. Xu, Scripta Mater. 55 (2006) 541.
[9] P.J. Hsieh, S.C. Lin, H.C. Su, J.S.C. Jang, J. Alloy Compd. 483 (2009) 40.
[10] Y.K. Xu, H. Ma, J. Xu, E. Ma, Acta Mater. 53 (2005) 1857.
[11] J.S.C. Jang, L.J. Chang, J.H. Young, J.C. Huang, C.Y.A. Tsao, Intermetallics 14 (2006) 945.
[12] P.Y. Lee, C. Lo, J.S.C. Jiang, J.C. Huang, Key Eng. Mater. 313 (2006) 25.
[13] J. Li, L. Wang, H.F. Zhang, Z.Q. Hu, H. Cai, Mater. Lett. 61 (2007) 2217.
[14] D.G. Pan, H.F. Zhang, A.M. Wang, Z.Q. Hu, Appl. Phys. Lett. 89 (2006) 261904.
[15] J.S.C. Jang, J.Y. Ciou, T.H. Hung, J.C. Huang, X.H. Du, Appl. Phys. Lett. 92 (2008) 011930.
[16] M. Kinaka, H. Kato, M. Hasegawa, A. Inoue, Mater. Sci. Eng., A 494 (2008) 29.
[17] L. Riester, R.J. Bridge, K. Breder, Mater. Res. Soc. Symp. Proc. 522 (1998) 45.